[16]Reference 7; Eq. (5) in this reference is similar to our Eq. (4).

[17]J. M. Ziman, *Principles of the Theory of Solids* (Cambridge U. P., London, 1964), pp. 278–9.

[18]Reference 14, pp. 21–22.

[19]A. D. Brailsford, Phys. Rev. 149, 456 (1966), Eq. (23).

[20]Reference 19, Eq. (40).

[21]Reference 19, Eq. (31).

[22]The design of our apparatus was influenced by a design of J. B. Ketterson and Y. Eckstein, Rev. Sci. Instr. 37, 44 (1966).

[23]R. W. Reed and F. G. Brickwedde, Rev. Sci. Instr. 39, 1216 (1968).

[24]This circuit was adapted from D. F. Gibbons and L. M. Falicov, Phil. Mag. 8, 177 (1963).

[25]R. Maddin and W. R. Asher, Rev. Sci. Instr. 21, 881 (1950).

[26]M. Levy and I. Rudnick, J. Acoust. Soc. Am. 34, 520 (1962).

[27]The field of the superconducting magnet in air and liquid helium is described by H, measured in oersteds. The conduction electrons in the specimen respond to B, measured in gauss. It was assumed that the relative permeability μ of Mg and the apparatus inside the superconducting solenoid was 1.

[28]The relation between the magnetoacoustic period $\Delta(1/B)$ and the corresponding extremal area S it measures is $\Delta(1/B) = 2\pi e/c\hbar S$ or $s_m = 2.673 \times 10^{-7} \Delta(1/B)$, if s_m is in a.u. and $\Delta(1/B)$ is in G^{-1}.

[29]R. W. Stark and L. M. Falicov, in *Progress in Low Temperature Physics*, edited by C. J. Gorter (North-Holland, Amsterdam, 1967), Vol. V, Chap. VI, pp. 235–286.

[30]Stark (Ref. 9) identified component frequencies of complex mixtures of harmonic oscillations in the dHvA effect using the field-modulation technique described by R. W. Stark and L. R. Windmiller, Cryogenics 8, 272 (1968).

[31]Dr. Stark has informed us that he has checked his determination of the μ_1^5 area and concluded that his original value is correct.

[32]Dr. Stark informed us that he also had observed this modulation of the λ oscillations in the dHvA effect.

[33]S. A. Friedberg, I. Estermann, and J. E. Goldman, Phys. Rev. 85, 375 (1952); 87, 582 (1952).

[34]Reference 19, Part IV.

[35]R. A. Phillips and A. V. Gold, Phys. Rev. 178, 932 (1969).

PHYSICAL REVIEW B VOLUME 3, NUMBER 4 15 FEBRUARY 1971

Ultrasonic Quantum Oscillations in Chromium†

D. F. Snider*‡§ and R. L. Thomas
Department of Physics, Wayne State University, Detroit, Michigan 48202
(Received 13 August 1970)

Measurements of quantum oscillations in the ultrasonic attenuation have been made to investigate the Fermi surface of chromium in the "single-$\vec{Q}$" state. Several frequency branches were followed over the entire Fermi surface and many of these data agree with earlier de Haas–van Alphen and ultrasonic results. Three branches display harmonic behavior which is exact when the measuring field is in the basal plane, but which deviates smoothly from exactness as the field is rotated toward $\vec{Q}$. The most likely explanation of this feature is that of magnetic breakdown among nonextremal orbits on the Fermi surface. The lack of degeneracy of the branches at certain symmetry axes prevented identifying the data with the location of sections of the Fermi surface. The data in one family of branches agree point by point with the de Haas–van Alphen results when the measuring field is near the basal plane, but differ as the field approaches $\vec{Q}$. For the remaining data, symmetry arguments may not be applicable because of changes in the topology caused by magnetic breakdown.

I. INTRODUCTION

The antiferromagnetic ground state of chromium has been successfully explained[1] in terms of spin-density wave (SDW) theory.[2] A central feature of this description is that the wave vector $\vec{Q}$ of the SDW is incommensurate with the lattice periodicity, and that a number of energy gaps are introduced into the band structure, giving rise to drastic changes in the Fermi-surface topology from that predicted for the paramagnetic state.

Below the Néel temperature T_N and without external constraints, the magnetic structure of normal chromium is cubic. However, if a relatively strain-free crystal is cooled through the Néel temperature in the presence of a sufficiently large magnetic field, only one SDW appears which is along the [100] axis nearest in orientation to the cooling field.[3,4] This is usually called the "single-$\vec{Q}$" state. In the temperature region $T_{sf} < T < T_N$ and in the presence of a magnetic field, chromium displays orthorhombic symmetry.[5,6] Here, T_{sf} is the spin-flip temperature at which the polarization of the SDW changes from transverse to longitudinal.[7] Below T_{sf}, chromium's magnetic symmetry is tetragonal, with fourfold rotational symmetry about

the $\vec{Q}$ vector.[8] For a strain-free and non-field-cooled chromium sample, there exist, below T_N, three SDW's oriented along the equivalent $\langle 100 \rangle$ axis. Experimental evidence for the $3\vec{Q}$ state is found in neutron diffraction experiments[9] which, however, do not distinguish between a model consisting of a collection of domains, each containing a single $\vec{Q}$ with random orientation among the $\langle 100 \rangle$ axes, and a model for which three mutually perpendicular macroscopic SDW's are postulated to coexist throughout the entire crystal. In either SDW model, the paramagnetic Fermi surface is truncated whenever $|\vec{k}| = |\vec{k}+\vec{G}+n\vec{Q}|$, where n is an integer indicating the order of $\vec{Q}$ involved in the transition, and $\vec{G}$ is a reciprocal-lattice vector. In the domain model, the Fermi surface is truncated by the energy gaps associated with a single SDW for both the single-$\vec{Q}$ and triple-$\vec{Q}$ states, so that the de Haas–van Alphen (dHvA) frequencies in the triple-$\vec{Q}$ state are merely a superposition of those present in the single-$\vec{Q}$ state. In the coexisting model, on the other hand, all three SDW's truncate the Fermi surface resulting in additional frequencies not seen in the single-$\vec{Q}$ state. A dHvA investigation indicated the domain model was correct.[10] Thus, in the antiferromagnetic region of chromium, the single-$\vec{Q}$ state may be regarded as fundamental.

The first investigation of the Fermi surface of chromium using the technique of ultrasonic quantum oscillations was reported by Wallace and Bohm (WB).[11] Quantum oscillations occur as the Landau levels pass through the Fermi surface periodically in $1/H$, where H is the magnetic field. When the electron mean free path is small in comparison with the sound wavelength, as is the case here, each frequency is proportional to an extremal cross-sectional area of the Fermi surface, just as for the dHvA technique. WB[11] observed quantum oscillations from 38 to 49 kG in the single-$\vec{Q}$ (field-cooled) state. Their measurements were taken in a plane defined by the field-cooling axis ($\parallel$ [001]) and a [100] axis, and also in the basal plane, normal to $\vec{Q}$. They observed several high-frequency branches in both planes which they interpreted in terms of sum frequencies or as harmonics of lower-frequency branches.

Graebner and Marcus (GM)[12] also investigated the antiferromagnetic state with dHvA-effect measurements. They obtained data throughout five symmetry planes with a maximum field of 33 kG, but their results typically did not agree with WB concerning harmonic behavior.

In the present work, the measurements of WB were repeated and extended, making use of digital data-acquisition techniques and improvements in the speed of numerical analysis. Much of the present data, taken in the region from 27 to 59 kG, agrees well with the results of WB and GM. Two harmonics and one sum-frequency branch, which were observed in this experiment, are in better agreement with WB than with GM. These frequencies are exact to within the estimated experimental error in the basal plane, as reported by WB, but depart smoothly from being exact as the magnetic field is rotated away from the basal plane. GM tested several frequencies for harmonic behavior but with negative results to within their estimated experimental error. The present work also differs with GM concerning the assignment of a particular family of branches to sections of a model Fermi surface.

II. EXPERIMENTAL

High-frequency sound waves are strongly attenuated by the conduction electrons in a pure metal at helium temperatures.[13] In the presence of a strong magnetic field, the energy states of the conduction electrons are quantized, with the result that the electronic density of states at the Fermi level periodically varies in $1/H$, where H is the magnetic field strength. The period of these variations is $2\pi e/\hbar c A_0$,[14] where A_0 is an extremal cross-sectional area of the Fermi surface normal to $\vec{H}$. This periodic variation of the density of states is reflected in the ultrasonic attenuation. For situations where $ql \gg 1$, where q is the ultrasonic wave number and l is the electron mean free path, the constraints of energy and momentum conservation in the electron-phonon scattering interaction can result in ultrasonic quantum oscillations which represent nonextremal Fermi-surface cross sections. In the present experiment, however, $ql < 1$ and all frequencies reported here are proportional to extremal areas.

The chromium single crystal used for this experiment has an irregular cross section which could contain an inscribed circle of maximum diameter of 0.255 in. and of approximate thickness 0.21 in. The large faces on which the transducer was bonded were approximately 4° from being normal to an $\langle 001 \rangle$ axis. The nominal purity was estimated to be better than 99.99%.

The crystal was field cooled by cooling it from 64 to 0 °C in a 60-kG field (the Néel temperature of chromium is 38.5 °C). During this operation the crystal was supported in a fixed sample holder so that the normal to a face was along the magnetic field direction. Despite the 4° misorientation of the face, the $\vec{Q}$ vector of the SDW lay along an $\langle 001 \rangle$ axis.[3] Neutron diffraction studies, following the experiment, indicated that the crystal was in a "single-$\vec{Q}$" state to better than 98%.

The standard pulse-echo technique was used.[11,13] The frequency of the shear sound waves propagated through the crystal was 110 MHz and the shear

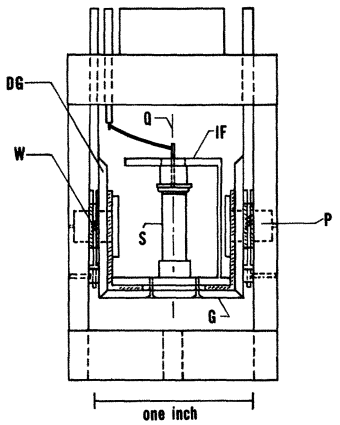

FIG. 1. Sketch of differential mechanism. Two drive shafts engaged worms W which turned two bevel gears DG. The frame IF which supported the sample S was fastened to a third bevel gear G forming a differential. When DG both turned in the opposite senses, IF rotated about Q, parallel to the SDW vector of the crystal used in this experiment. When DG turned in the same sense, IF rotated about P, the analog of the x axis of Fig. 2.

polarization was along a ⟨110⟩ axis. All the data were taken at 1.1 °K.

The crystal could be rotated with two degrees of freedom by means of a sample holder[15] which is illustrated in Fig. 1. This holder permitted data to be recorded at angular orientations corresponding to intersections of longitude and latitude lines on a sphere.

One dc signal proportional to the relative sound attenuation and another proportional to the magnetic field strength were alternately sampled by a digital acquisition system[16] and the values punched on paper tape for computer processing. Each run resulted in 3000 pairs of points with at least three points sampled per oscillation for the fastest frequency. The highest frequency which could be resolved was 40×10^6 G.

Angular orientations of the crystal at which data were recorded are specified by the angles θ and ϕ, where θ ranged from 0 to 90° in 10° increments, and ϕ ranged from 0 to 40° in 10° increments, as well as for $\phi = 45°$. In this notation, θ indicates the polar angle from $\vec{Q}$ ($\parallel$[001]), and ϕ is the azimuthal angle between a ⟨100⟩ axis in the plane of the crystal and a reference axis in a plane perpendicular to the field (see Fig. 2). For comparison with GM, the planes B, C, and D are $\phi = 45°$, $\phi = 0°$, and $\theta = 90°$, respectively. In order to establish accurately the symmetry directions, the crystal orientation was rotated at constant field strength at liquid-helium temperature. The location of extrema in attenuation for this rotation pattern indicated the twofold and fourfold symmetry directions. Following this rough alignment, the fine orientation was made by analyzing data for symmetrically located pairs of points. The final orientation is estimated to be accurate to within 0.5°. After the orientation was established, the sample was kept continuously at liquid-helium temperature to insure the integrity of the transducer bond. The field was measured by a NMR-calibrated bismuth magnetoresistive probe, and the calibration table was incorporated into the computer program.

The data were converted from punched tape to cards and processed on an IBM 360/65 computer. The raw signal was preprocessed by the computer to correct for receiver nonlinearities and to interpolate the data for field values corresponding to equal spacing in $1/H$. In addition, slowly changing frequencies were removed from the signal by assuming the background to be linear over the experi-

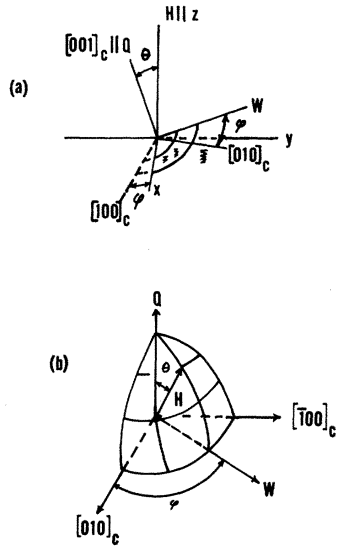

FIG. 2. Coordinate systems used in taking data. Two coordinate systems are displayed in (a). The axes relative to the fixed magnetic field are x, y, and z. The crystal axes are bracketed with the subscript c. The magnetic field H is parallel to the z axis and, in (a), $\vec{Q}$ is shown rotated an angle θ around the x axis from H. Because $\vec{Q}$ is along the crystal's [001] axis, $\vec{Q}$ always lies in the yz plane. The crystal can also be rotated about $\vec{Q}$, and ϕ is the angle between the crystal's [100] axis and x. If $\vec{Q}$ is rotated away from $\vec{H}$, the basal plane and the xy plane are not coplanar. The basal plane is defined by $[100]_c$ and $[010]_c$ and includes $\vec{x}$ and $\vec{W}$, the intersection of the basal plane with the yz plane. In the crystal's coordinate system shown in (b), the magnetic field moves in the plane defined by $\vec{Q}$ and $\vec{W}$ and ϕ may be considered, equivalently, as the angle between the crystal axis $[010]_c$ and $\vec{W}$. Data points are recorded at intersections of curves of longitude and latitude as indicated.

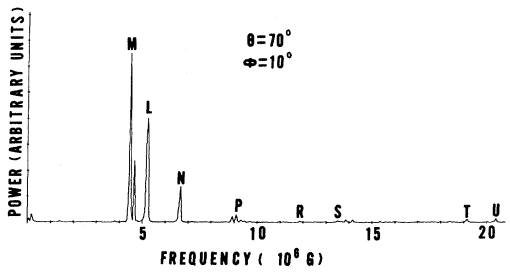

FIG. 3. Tracing of a typical power spectrum. Here $\theta = 70°$, $\phi = 10°$, and the letters correspond to frequencies listed in Table I.

mental field range and subtracting a least-square linear fit from the raw data. The main program then determined the power spectrum using a fast Fourier algorithm.[17] Prior to the transform, the data were multiplied by an appropriate cosine "window" to improve the fidelity of the power spectrum.[18] Each subroutine of the program was checked by hand calculations, and in addition, computer-calculated data were compared with an experimental dHvA run on a potassium sample to test the system as a whole for an accurately known quantum oscillation frequency.[19]

III. RESULTS

The raw data for each angular orientation were processed to give the amplitude of each frequency component in equal increments and the power spectrum was displayed both in tabular form and as a Calcomp plot. A typical power-spectrum plot is displayed in Fig. 3. The frequency peaks were located roughly on the plots and identified more precisely from the tabular read out. The strongest frequencies were then plotted as smooth branches in equal increments of either θ or ϕ. Because each point was a member of a constant θ branch as well as a constant ϕ branch, the requirements of smoothness and continuity on both branches considerably reduced the number of possible connections (see Fig. 4). For example, choices in the connection of a point on the constant θ branch were rejected which resulted in a cusp in the constant ϕ branch through the same point, or which resulted in a branch shape that changed drastically in adjacent curves. Values of the frequencies sufficiently strong to be followed over at least a moderate angular range are listed in Table I.

The strength and the percentage accuracy of the Calcomp peaks depended on the frequency range, as did the reliability of forming the connections among the data points. Above 25×10^6 G, peak heights were smaller and less well defined than in the midfrequency range. Frequencies in the range $1-3\times10^6$ G were weak and appeared for only a few orientations. Strong peaks were present in the region 0.6×10^6 G, but the resolution of the program was inadequate to assign accurate values. Because of the way in which the Fourier transform was computed, the power spectrum was evaluated at integral multiples of a suitably small frequency. As a result, the percentage error was rather large in the region of the low-frequency peaks. These low frequencies, however, were also not sufficiently strong to be identified by hand analysis of the raw data. The most reliable data from this experiment are therefore in the frequency range $4-18\times10^6$ G.

The crystal orientation (and hence the orientation of $\vec{Q}$) relative to the measuring field is estimated to be accurate to within 0.5° and the orientation of the sound wave vector $\vec{q}$ is within 4° of the [001] direction. The reproducibility of the frequency spectra as judged by comparing data from symmetrical orientations was 0.5%. However, some small peaks did not reproduce in symmetrical orientations, probably because of the influence of line shape in identifying a peak in the power spectrum.

The convention adopted in labeling the curves of the data will be the use of capital letters near the end of the alphabet. Capital letters at the beginning of the alphabet will denote the plane of the measuring field as used by GM. The notation used in labeling data by other workers will be followed here: subscripted lower-case letters for WB and lower-case Greek letters for GM. Our data are plotted together with these earlier results in Figs. 5–7.

Within the plane "*B*" of GM (Figs. 7 and 8), the frequency *L* agrees well with GM over the entire region. Frequency *N* also agrees over the range $30° \leq \theta \leq 90°$ but for $\theta < 30°$ there is a difference in connections. GM report no branches corresponding to our branches labeled *P* and *R*. Branch *S* of the present data agrees well for $70° \leq \theta \leq 90°$ with the

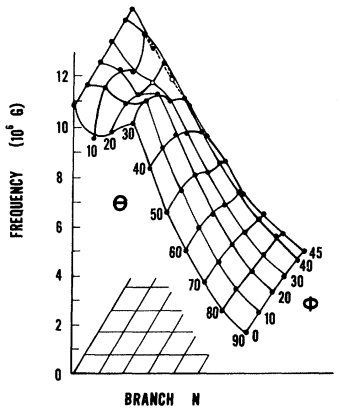

FIG. 4. Surface of the frequency *N* for both polar and azimuthal angles (in deg).

corresponding curve of GM. The points on branch U are coincident with the GM branch μ for $10° \leq \theta \leq 30°$. At $\theta = 0°$, the connections among our data can not be made unequivocally and the curve μ of

TABLE I. Frequency branches vs angle. The superscript e indicates the value was estimated from the connection curves.

Angle		Frequency branches (10^6 G)							
θ	ϕ	L	M	N	P	R	S	T	U
0	0	8.66	10.85	10.85	15.36	17.85	17.85	17.85	17.85
10	0	7.40	8.28	9.98	15.73		15.73		20.41
	10	7.40	8.30	11.10	14.86		16.18	18.74	19.58
	20	7.43	8.87	10.91	13.37		16.73		18.17
	30	7.54	8.92	10.03	14.41				18.5^e
	40	7.61	9.93	10.65	14.43	17.24	17.24		17.24
	45	7.70	9.62	9.62	15.00	16.29	16.29		16.29
20	0	6.50	7.11	10.66	13.73		13.73		20.60
	10	6.50	7.04	10.91	13.48		16.26	18.69	20.58
	20	6.59	7.67	10.37	11.87		16.90		18.70
	30	6.61	8.05	10.0^e	13.3^e				19.72
	40	6.65	8.7^e	9.95	13.24	16.29	16.30		16.29
	45	6.67	8.8^e	8.8^e	13.27	15.78	15.78		17.38
30	0	5.94	6.48	11.47	11.47	15.91	13.69	19.99	21.61
	10	5.90	6.49	11.45	11.45		15.53	18.18	19.96
	20	5.92	6.75	10.81	10.82		17.63		18.70
	30	5.91	7.36	9.71	12.06		15.99		21.47
	40	5.93	7.89	8.93	11.86	14.80	14.80		18.40
	45	5.91	8.16	8.16	11.89	14.08	14.08		18.58
40	0	5.50	5.50	10.05	11.07	14.18	14.18		20.82
	10	5.51	5.51	9.96	10.91		15.35	17.03	19.68
	20	5.50	6.15	9.62	10.99		15.95		17.38
	30	5.44	6.46	8.82	10.88	13.05	14.38		20.37
40	40	5.40	6.99	8.04	10.86	13.37	13.37		20.00
	45	5.40	7.26	7.26	10.80	12.98	14.27		19.73
50	0	5.27	5.27	8.63	10.30	12.82	14.67		20.0^e
	10	5.31	5.31	8.62	10.56		14.69	17.94	19.30
	20	5.22	5.23	8.29	10.69		15.56		18.44
	30	5.17	5.89	7.69	10.33	12.86	14.72		18.80
	40	5.07	6.24	7.15	10.21	12.23	13.94		20.54
	45	5.06	6.53	6.79	10.12	11.85	14.09		19.09
60	0	5.22	4.68	7.56	9.36	12.72	14.94	19.08	20.28
	10	5.19	4.71	7.56	9.76	12.65	13.84		20.32
	20	5.09	5.09	7.27	10.25	12.40	14.61		18.03
	30	5.04	5.00	6.78	9.97	11.79	13.72		18.26
	40	4.89	5.69	6.36	9.79	11.26	13.83		19.27
	45	4.80	5.88	5.88	9.66	10.94	13.75		18.61
70	0	5.20	4.57	6.72	8.96	11.90	15.39	19.32	20.44
	10	5.23	4.45	6.65	9.09	11.83	13.49	19.14	20.39
	20	5.14	4.66	6.45	10.21	11.59	13.32		18.58
	30	4.95	4.96	6.10	9.49	11.07	13.60		17.35
	40	4.83	5.25	5.74	9.84	10.57	13.99		18.08
	45	4.79	5.43	5.43	9.52	10.29	13.74		18.60
80	0	5.40	4.32	6.05	8.57	11.39		18.05	21.47
	10	5.37	4.48	6.02	8.67	11.32	13.27	18.11	21.30
	20	5.22	4.38	5.88	8.75	11.10	13.74		20.81
	30	5.01	4.77	5.62	9.48	10.63	13.59	16.36	19.02
	40	4.85	4.86	5.35	9.71	10.14	13.71	15.67	18.75
	45	4.78	5.15	5.15	9.50	9.50	14.10	15.08	18.57

TABLE I. (*continued*)

Angle		Frequency branches (10^6 G)							
θ	ϕ	L	M	N	P	R	S	T	U
90	0	5.63	4.25	5.63	8.50	11.25	13.7[e]	17.96	22.57
	10	5.56	4.26	5.56	8.70	11.19	13.73	16.81	22.43
	20	5.46	4.38	5.45	8.76	10.92	13.80	16.20	21.96
	30	5.22	4.51	5.23	9.14	10.24	14.05	15.44	21.96
	40	5.00	4.70	5.00	9.40	10.01	14.17	14.90	20.59
	45	4.88	4.88	4.88	9.76	9.76	14.52	14.52	19.10

GM stops for $\theta > 40°$.

In plane "*C*" (Figs. 5, 7, and 9), branch L agrees with GM over the entire plane and with WB (b_{21}) from 10° until 90°. Except at $\theta = 0°$ ($\vec{H} \parallel [001]$), branch M also fits WB (b_1) for $20° \leq \theta \leq 90°$ and GM for $10° \leq \theta \leq 90°$. The WB data end at 20° and there is a difference with GM as to the correct branch connection at $\theta = 0°$. Curve N coincides with both GM and WB (b_{22}) for $40° \leq \theta \leq 90°$. The data of WB end at 30° and the branch of GM ends at 40° so that a further comparison cannot be made. Curve P agrees with WB (c_1) in the range $50° \leq \theta \leq 90°$ but with scatter which is larger than the estimated experimental error. The agreement is only qualitative with GM through $30° \leq \theta \leq 90°$. No curve of GM corresponds to our branch R, but several points on R fall on the curves c_2 or c_3 of WB.

In the basal plane "*D*" (Figs. 6, 7, and 10), branches M and L match GM and WB (b_1 and b_2, respectively) throughout the entire plane. Our branch P lies within experimental uncertainty of both WB (branch c_1) and GM (branch θ). Branch R is coincident with WB branch c_2 with no corresponding branch in the GM results. The curve Q may correspond to the curve c_3 of WB but quantitative agreement is poor. GM have no corresponding points. Except for $\phi = 0°$ ($\vec{H} \parallel [001]$), our branch T fits WB (d_2) but is consistently higher than GM (λ). Our lower branch S is in good agreement with GM but lies above the branch d_1 of WB. Among the remaining data, isolated points coincide with either GM or WB but there is not a sufficiently clear trend to establish additional branches.

IV. DISCUSSION

Summarizing the general features of the data, many sections are in quantitative agreement with the results of GM and WB. Systematically, however, departures from agreement are most pronounced as the measuring field approaches the $\vec{Q}$ direction. It is assumed here that the dHvA and ultrasonic oscillations under comparison represent extremal cross-sectional areas of the Fermi surface but that because of the different physical mech-

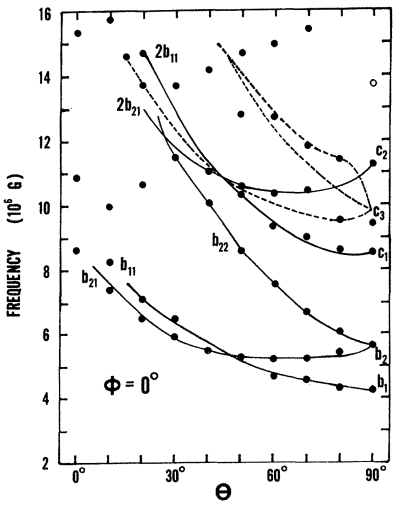

FIG. 5. Data for this work superimposed on the data of WB in the plane containing $\vec{Q}$ and the [100] axis (plane *C*). The data of WB are shown as lines, and our data as solid circles. The error in transcribing the data of WB is approximately equal to the diameter of our dots.

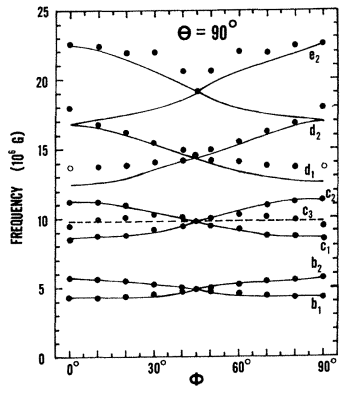

FIG. 6. Data for this work superimposed on the data of WB in the basal plane (plane *D*). The data of WB are shown as lines, and our data as solid circles. The error in transcribing the data of WB is approximately equal to the diameter of our dots.

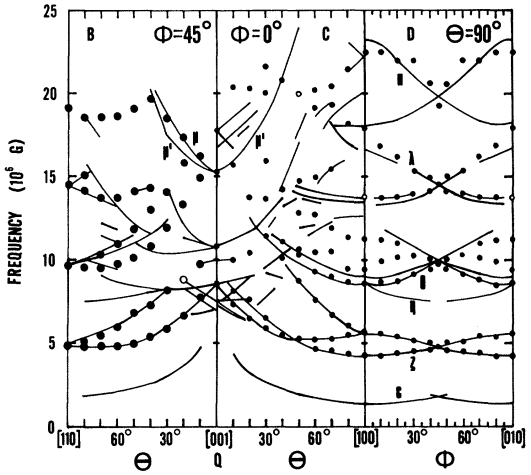

FIG. 7. Data for this work superimposed on the data of GM. The data of GM are shown as lines, and our data as solid circles. The error in transcribing the data is approximately equal to the diameter of our dots. The data of plane *B* were obtained from Fig. 13 of Graebner's thesis; planes *C* and *D*, from Fig. 11.

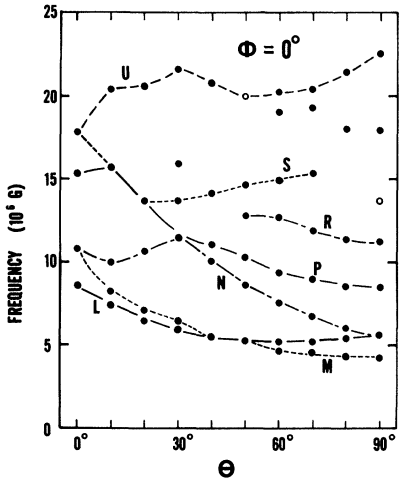

FIG. 9. Frequencies vs angle. Plane includes $\vec{Q}$ and the [100] axis. This plane corresponds to the plane labeled *C* of GM.

anisms which are involved, the relative amplitudes for various orbits may differ markedly for the two techniques. Such considerations of experimental sensitivity may account for curves observed by GM but not by either WB or the present work, and vice versa. If this apparent discrimination by the two techniques is indeed real, the two experimental approaches are complementary – a useful feature for investigations of a Fermi surface as complex as that of chromium.

In the analysis of their data, WB found that several higher branches were expressible as sum frequencies or as harmonics of lower branches. GM, however, found harmonic behavior in only one branch μ_2 ($\mu_2 = 2\mu$), and observed no sum frequencies. The data reported here manifest both sum frequencies and harmonics. Except for the point at $\phi = 0°$, the branch *T* equals 3*N* to within 1.5% in the basal plane (see Table I), slightly more than

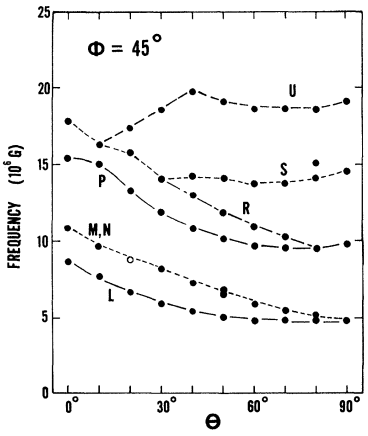

FIG. 8. Frequencies from extremal cross-sectional areas of the Fermi surface vs orientation of the magnetic field. Angle indicated is the angle between $\vec{Q}$ along the [001] axis, where $\theta = 0°$, and the measuring field in a plane containing $\vec{Q}$ and the [110] axis. This plane corresponds to the plane labeled *B* of GM. Open circles correspond to points estimated from the connection curves.

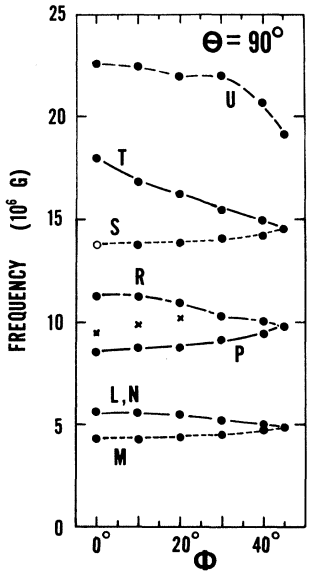

FIG. 10. Frequencies vs angle. Polar angle is 90° and the measuring field lies in the basal plane. This plane corresponds to the plane labeled *D* of GM. Crosses are points lying on the curve *Q* mentioned in the text.

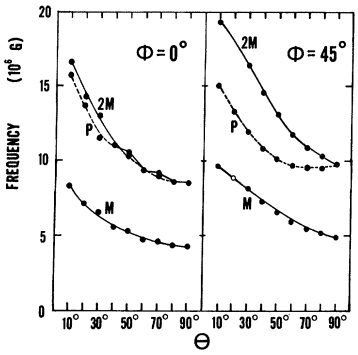

FIG. 11. Variation of harmonic behavior with polar angle for the frequency curve P. The lowest solid curve is the base frequency M; the middle dashed curve, the experimental data P; and the upper solid curve $2M$. Note the smooth variation as the measuring field leaves the basal plane and that the rate of departure from harmonicity varies with the azimuthal angle.

the estimated experimental uncertainty (1%) for the difference $3N-T$. The branch P is twice the frequency M to within 2% in the basal plane. The departure from apparent harmonicity gradually increases as the measuring field leaves the basal plane (see Fig. 11). For example, at $\theta = 80°$ the deviation ranges from less than experimental error to 8.1% and at $\theta = 70°$, from 2% to 13.6%. For fixed θ, the deviation increases with ϕ to a maximum at $\phi = 45°$. Except for three points, the frequency R is the sum of frequencies N and L (see Table I) in the interval $60° \leq \theta \leq 90°$ for all values of ϕ, to within experimental error. The deviation from an exact sum exceeds the experimental error for $\theta < 60°$ (see Fig. 11). The branch P is a harmonic for a smaller range than the sum frequency R. Within the basal plane, P lies between curves of GM and WB, but R matches WB results closely and is significantly lower than the nearest branch of GM in the basal plane. No counterpart for this branch appears in GM for the plane C.

Another feature of the data is the behavior of frequency branches at symmetry axes. GM have interpreted their dHvA data from these points making use of certain symmetry arguments and have tentatively identified some of these data with sections of a model Fermi surface. Although the present raw data themselves exhibit the proper tetragonal symmetry, the frequency branches do not possess degeneracies along symmetry axes which conform to the alternatives presented by GM and which were used to deduce their Fermi-surface assignments. The differences between our connections and those of GM may result from the different field regions used in the two experiments.

One physical mechanism which is sometimes invoked to explain harmonic behavior is that of Landau-level spin splitting. The spin orientation of an electron in an external magnetic field removes the twofold degeneracy of the Landau energy levels. Experimentally, this can result in spin splitting of the quantum oscillations in the ultrasonic attenuation and can also introduce harmonics of the unperturbed quantum oscillations.[20,21] This is reflected formally in the theoretical expression[22] for the attenuation coefficient γ:

$$\frac{\gamma}{\gamma_0} = 1 + \sum_{n=1}^{\infty} (-1)^n \frac{4\pi kT}{\hbar\omega} \sin\left(\frac{n\omega}{\omega_c}\right) \cos\left(\frac{g\pi nm^*}{2m}\right) \times \frac{\cos(2\pi n\zeta_0/\hbar\omega_c)}{\sinh(2\pi^2 nkT/\hbar\omega_c)}, \quad (1)$$

where γ_0 is the zero-field attenuation, ω the angular sound frequency, ω_c the cyclotron frequency, T the absolute temperature, and ζ_0 the Fermi energy. The spin term is $\cos(g\pi nm^*/2m)$, where m^* is the cyclotron mass and g the spectroscopic g factor of the conduction electrons. If $\hbar\omega_c \gg kT$, i.e., if the Landau-level separation is much larger than the thermal broadening of the levels, several terms may contribute to the sum. For example, if $g \sim 2$ and $m^*/m \sim \frac{1}{2}$, the cosine term is small for both $n = 1$ and $n = 3$, so that the ratio of the second harmonic to the first can be large. This argument has been proposed to account for harmonic content in dHvA data for cadmium.[23] As has been mentioned previously, the harmonic content of our data is very strongly angular dependent, being most pronounced in the basal plane (normal to $\vec{Q}$). If gm^*/m varies with orientation, harmonic content introduced by possible spin splitting would change correspondingly. In chromium, m^* is rather isotropic,[12] and hence if spin splitting is to account for the present results, g must be rather anisotropic. There is experimental evidence in the case of platinum[24] to suggest that variations in g are of the same order of magnitude as those in m^*. If this is true generally, spin splitting is not likely to explain the harmonic behavior in chromium. In zinc, where spin splitting has been studied thoroughly, even though g and m^* are anisotropic,[25,26] the product $gm^*/2m$ is independent of angle.[27] Furthermore, although dHvA results in Cd and Zn which display harmonic behavior have been interpreted in terms of spin splitting, there does not seem to be any evidence in those investigations for the presence of sum or difference frequencies, whereas sum frequencies are observed in the present data.

Another possible explanation for harmonic content is the so-called "B-H" effect first discussed by Shoenberg.[28] The magnetic field "seen" by the electrons inside the metal is B, the magnetic induction, and the proper inclusion of the sample's internal magnetization can result in sum and dif-

ference frequencies as well as harmonics.[29] In two dHvA investigations,[30,31] a difference frequency was also observed which is consistent with harmonic distortion.[29] The present data, however, displayed no difference frequency within the frequency range scanned. The experimental signal was quite complicated but the sawtooth shape of the oscillations characteristic of the B-H effect[30,32,33] also was not apparent in the present data. For the case of ultrasonic attenuation, however, the attenuation coefficient is not transcendental in the magnetization [cf. Eq. (1)], so that there is no "feedback" between the left and right sides of the equation. As a consequence, the B-H effect may not be a significant source of harmonics in this experiment.

Instrumental effects are also unlikely as a source of harmonics. Nonlinearities in the electronic equipment, although certainly present, would be expected to produce harmonics which are exact for all branches over all angular orientations. However, in the present data, harmonic behavior appeared in three branches for only limited angular regions with a smooth departure from exactness for other orientations.

Perhaps the most likely explanation of harmonic content in the present data involves the possibility of magnetic breakdown orbits.[34] New frequencies can arise when an electron moving in an intense magnetic field tunnels through energy gaps separating adjacent sections of the Fermi surface and follows an orbit traversing each section. Orbits in an hexagonal-close-packed metal, for example, can be practically exact harmonics and sum frequencies of smaller orbits.[34] It has also been observed experimentally that magnetic breakdown can connect nonextremal areas.[35] The breakdown orbit itself must be extremal, but whether this condition occurs when each individual cross section is extremal is dependent upon the Fermi-surface geometry. Sections of the Fermi surface could be situated so that at one magnetic field orientation the extremal breakdown orbit between two surfaces would be a sum of the extremals from each surface, but at a second orientation of lower symmetry, the extremal combined orbit does not link orbits which themselves are extremal. These aspects of magnetic breakdown could account for several features of the present data. The Fermi-surface geometry, for example, could be such that in the basal plane, the orientation of highest symmetry, the sum frequency is exactly the sum of two lower-frequency branches and the harmonics are also exact. As the measuring field is rotated out of the basal plane towards $\vec{Q}$, the geometry for the cross sections changes and the sum frequency and harmonics are no longer observed to be exact. This could correspond to magnetic breakdown linking nonextremal orbits in the lower-symmetry experimental situation. The rate at which the deviation from an exact sum or harmonic increases with angle is observed to depend upon the particular branch: For example, at $\theta = 70^\circ$ the branch T may be further from a harmonic than is branch P, or than is branch R from being an exact sum. Because the probability of breakdown increases with magnetic field strength, breakdown effects of the sort suggested here would be more likely to appear in these data than in the data of GM, resulting in a slightly different spectrum of frequencies for the two experiments. Furthermore, magnetic breakdown in chromium's magnetoresistance has been observed experimentally at an approximate field strength of 50 kG.[36–38]

The differences in connections at symmetry axes between these results and the data of GM and the usefulness of degeneracy in locating pieces of the Fermi surface represent two other points of disagreement which must be considered. It seems pertinent in light of the previous discussion to view these differences also within the framework of magnetic breakdown effects. Consider, for example, a Fermi surface which has tetragonal symmetry about a $\langle 001 \rangle$ axis. Let us assume also, for simplicity, that one piece of the Fermi surface is an ellipsoid of revolution which is located a distance $\vec{b}$ from the origin along the [100] direction. Symmetry then requires that identical ellipsoids also be located a distance $\vec{b}$ from the origin along the $[\bar{1}00]$, [010], and $[0\bar{1}0]$ directions. When the measuring field is directed along the [100] direction, there are two extremal cross sections with two resulting frequencies. One frequency arises from the elliptical cross section of two of the ellipsoids and the other from the circular cross section of the other two ellipsoids. However, if the measuring field is along the [110] direction, all ellipsoids are seen symmetrically. For $\vec{H} \| [001]$, then, the extremal cross sections are identical and the frequency branches coalesce. A generalization of such an argument was used by GM to deduce the degeneracy of the frequency branches at symmetry axes and to relate these branches to sections of the Fermi surface located at symmetry points in the Brillouin zone.

Much of the present data can be followed over the entire Fermi surface, but our data in GM's planes B, C, and D do not satisfy their degeneracy relations (see Fig. 7) at the high-symmetry axes. Our connections are perhaps more reliable than those of GM because the data were taken over the entire Fermi surface. On the other hand, GM took more data in the symmetry planes to which their measurements were restricted and their curves for those planes are more complete. We disagree, in particular, with GM regarding the degeneracy of their curves labeled ζ along the [001] axis (see Fig. 7). Our data (curves L, N, M) agree point by

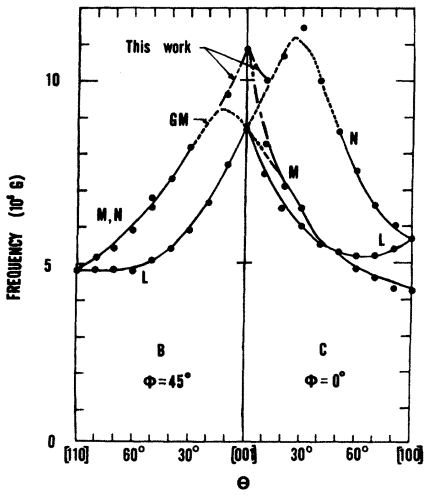

FIG. 12. Data for this work superimposed on the data of GM. The data of GM are shown as solid lines and their extrapolations as broken lines. Our data are drawn as solid circles, and our branches as dashed lines. The error in transcribing the data is approximately equal to the diameter of our dots. The data of plane *B* were obtained from Fig. 13 of Graebner's thesis; planes *C* and *D*, from Fig. 11.

point with the curves ζ in planes *B* and *C* in the angular region $40° \leq \theta \leq 90°$ and $30° \leq \theta \leq 90°$, respectively, and in that region our frequency curves overlap. For $\theta \leq 30°$, however, their data stop and are extrapolated in both planes to $\vec{H} \parallel [001]$ to infer the connections there. As has been pointed out earlier, the degeneracy along symmetry axes is crucial in identifying the location of a section of the Fermi surface using symmetry arguments. GM assert that the curves coalesce along the [001] axis as is necessary for their Fermi-surface assignment. However, our corresponding three curves do not meet at $\vec{H} \parallel [001]$, but instead cross this axis at two distinct places (see Fig. 12). This separation is seen repeatedly throughout all our planes containing the [001] axis (for example, see Fig. 8 and Table I). Moreover, our curves were formed directly, without extrapolation. If the frequency curves are nondegenerate at the [001] axis, as the present data suggest, the location of this section of the Fermi surface which GM infer is not likely to be correct. A possible explanation for the fact that the remainder of our branches do not satisfy the GM degeneracy relations at the symmetry axes lies in their assumption that the surfaces are simple and closed; i.e., that only one frequency branch exists at each angular orientation from each closed section of the Fermi surface, and that the resulting frequency curves are continuous for all orientations. These assumptions prove to be rather stringent. For example, the dumbbell-model Fermi surface of Pippard[39] centered at the origin Γ with the axis of revolution along [001] possesses tetragonal symmetry and continuous frequency curves but does not have the degeneracy of a simple surface centered at Γ. Although several sections of the Fermi surface of paramagnetic chromium are likely to satisfy the assumptions of being simple and closed, the topology will be considerably different for the antiferromagnetic Fermi surface, especially at high fields where magnetic breakdown effects are important.

V. CONCLUSIONS

At the outset of this investigation, a discrepancy existed between the results of GM and WB regarding the presence of harmonic and sum frequencies. Clarification of this behavior was one motivation for performing the present work. Another was the limitation of the existing ultrasonic-attenuation measurements to two planes. It was hoped that additional data taken at appropriate orientations could not only define the Fermi surface more completely but also indicate the appropriate connectivity. Moreover, the technique of ultrasonic attenuation may provide additional information not available using other methods.

To summarize our results, the ultrasonic quantum oscillations investigated in this work have provided additional experimental information describing the Fermi surface of chromium in the single-$\vec{Q}$ state. We have compared the results of this investigation with the preliminary ultrasonic experiments of WB and also with lower-field dHvA measurements of GM. We conclude that the discrepancy between these two experiments is probably an effect of magnetic breakdown. We suggest that this mechanism could also explain why certain branches have a pronounced harmonic behavior which becomes progressively less exact as the measuring field is rotated away from the basal plane. This angular dependence could come about from magnetic breakdown orbits which themselves are extremal but which link individually nonextremal cross sections of the Fermi surface. For some frequencies the present results disagree with GM regarding branch connections, particularly when the measuring field is parallel to $\vec{Q}$. Consequently, we conclude that the tentative assignment of such data by GM to a model Fermi surface, which depends logically on the type of degeneracy of branches near this symmetry direction, may be incorrect. This conclusion is independent of the possible effects of magnetic breakdown since the individual data in question agree over much of the symmetry planes, but the connections among those data deduced in the present work were under the additional constraint of data obtained for orthogonal branches.

Because of the complexity of all the results ob-

tained to date, it is apparent that improved theoretical band-structure calculations will be necessary as a guide to interpre ..ie experimental data. An approach of this kind, although admittedly of a long-range nature, could result in a realistic Fermi surface and a better understanding of the ground state of chromium. Because of the apparently unique status of the SDW antiferromagnetism, we feel that, despite the complexity, such a program would be worthwhile, and it is hoped that the present experimental work will contribute to its motivation.

ACKNOWLEDGMENTS

The authors are grateful to Dr. S. Werner of the Ford Scientific Laboratory for neutron diffraction of the chromium crystal used in this work and to the Wayne State University Computing and Data Processing Center for machine time. Special thanks go to M. Monroe and M. Lefkofsky for liaison and technical advice. We also appreciate the assistance of M. Shopnick in the construction of the sample holder.

---

†Research sponsored by the U.S. Air Force of Scientific Research, Office of Aerospace Research, under AFOSR Grant No. 68-1494.

*This paper is based on a thesis submitted by D. F. Snider in partial fulfillment of the requirements for a Ph.D. degree at Wayne State University, Detroit, Mich.

‡Recipient of a National Aeronautics and Space Administration Traineeship.

§Present address: Osaka University, Osaka, Japan.

[1]For a recent survey, see, for example, L. M. Falicov and M. J. Zuckermann, Phys. Rev. 160, 372 (1967).

[2]A. W. Overhauser, Phys. Rev. 128, 1437 (1962).

[3]J. E. Graebner, Ph.D. dissertation, Northwestern University, Evanston, Ill., 1968 (unpublished).

[4]A. Arrott, S. A. Werner, and H. Kendrick, Phys. Rev. Letters 14, 1022 (1965).

[5]E. W. Lee and M. A. Asgar, Phys. Rev. Letters 22, 1436 (1969).

[6]M. O. Steinitz, L. H. Schwartz, J. A. Marcus, E. Fawcett, and W. A. Reed, Phys. Rev. Letters 23, 979 (1969).

[7]G. Shirane and W. J. Takei, J. Phys. Soc. Japan Suppl. 17, 35 (1962).

[8]B. R. Watts, Phys. Letters 10, 275 (1964).

[9]A. Arrott, in *Magnetism*, edited by G. T. Rado and H. Suhl (Academic, New York, 1966), Vol. II B, p. 295.

[10]J. Graebner and J. A. Marcus, J. Appl. Phys. 37, 1262 (1966).

[11]W. D. Wallace and H. V. Bohm, J. Phys. Chem. Solids 29, 721 (1968).

[12]J. E. Graebner and J. A. Marcus, Phys. Rev. 175, 659 (1968).

[13]For a review article, see, for example, N. Tepley, Proc. IEEE 53, 1586 (1965).

[14]L. Onsager, Phil. Mag. 43, 1006 (1952).

[15]G. F. Brennert, W. A. Reed, and E. Fawcett, Rev. Sci. Instr. 36, 1267 (1965).

[16]Vidar Corporation, Model 5200 D-DAS.

[17]C. Bingham, M. D. Godfrey, and J. W. Tukey, IEEE Trans. Audio Electroacoust. AU15, 2 (1967); 15, 56 (1967).

[18]R. B. Blackman and J. W. Tukey, *The Measurement of Power Spectra* (Dover, New York, 1958).

[19]R. L. Thomas and G. Turner, Phys. Rev. 176, 768 (1968).

[20]A. Myers and J. R. Bosnell, Phys. Letters 17, 9 (1965).

[21]Y. Shapira, Phys. Rev. Letters 13, 162 (1964).

[22]Sergio Rodriguez, Phys. Rev. 130, 929 (1963).

[23]Alexander D. C. Grassie, Phil. Mag. 9, 847 (1964).

[24]L. R. Windmiller and J. B. Ketterson, Phys. Rev. Letters 21, 1076 (1968).

[25]Alan J. Bennett and L. M. Falicov, Phys. Rev. 136, A998 (1964).

[26]A. S. Joseph and W. L. Gordon, Phys. Rev. 126, 489 (1962).

[27]J. R. Lawson and W. L. Gordon, in *Proceedings of the Ninth International Conference on Low Temperature Physics, Columbus, Ohio*, 1964, edited by J. G. Daunt, D. V. Edwards, F. K. Milford, and M. Yaqub (Plenum, New York, 1965), Vol. B, p. 854.

[28]D. Shoenberg, Phil. Trans. Roy. Soc. (London) A255, 85 (1962).

[29]D. Shoenberg, Can. J. Phys. 46, 1915 (1968).

[30]A. S. Joseph and A. C. Thorsen, Phys. Rev. 138, A1159 (1965).

[31]D. Shoenberg, Can. J. Phys. 46, 1925 (1968).

[32]A. B. Pippard, Proc. Roy. Soc. (London) A272, 192 (1963).

[33]J. H. Condon, Phys. Rev. 145, 526 (1966).

[34]See, for example, R. W. Stark and L. M. Falicov, in *Progress in Low Temperature Physics*, edited by C. J. Gorter (Wiley, New York, 1967), Vol. V, p. 235.

[35]R. C. Young, Phys. Letters 30A, 510 (1969).

[36]A. J. Arko, J. A. Marcus, and W. A. Reed, Phys. Letters 23, 617 (1966).

[37]A. J. Arko, J. A. Marcus, and W. A. Reed, Phys. Rev. 176, 671 (1968).

[38]A. J. Arko, J. A. Marcus, and W. A. Reed, Phys. Rev. 185, 901 (1969).

[39]A. B. Pippard, *Dynamics of Conduction Electrons* (Gordon and Breach, New York, 1965), p. 103.